

Angular anisotropy in pre-fission neutron spectra and PFNS of $^{240}\text{Pu}(n, F)$

V. M. Maslov¹

220025 Minsk, Byelorussia

Angular anisotropy of secondary neutrons was evidenced in neutron emission spectra (NES) of $^{239}\text{Pu}+n$ in 1972, and prompt fission neutron spectra (PFNS) of $^{239}\text{Pu}(n, F)$ in 2019, it might be predicted for $^{240}\text{Pu}(n, F)$ PFNS now. In case of NES angular anisotropy is due to direct excitation of collective levels and pre-equilibrium/semi-direct (states in the continuum are excited) mechanism of neutron emission of first neutron in $(n, nX)^1$ reaction, while in case of PFNS it is due to exclusive spectra of pre-fission neutrons of $(n, xnf)^{1\dots x}$ reactions. In $^{239}\text{Pu}(n, xnf)$ and $^{240}\text{Pu}(n, xnf)$ reactions observed PFNS envision different response to the emission of first pre-fission neutron in forward or backward semi-spheres with respect to the momentum of incident neutrons. Since energies of $(n, n_f)^1$ neutrons and their average values $\langle E_{nnf}(\theta) \rangle$ depend on angle of emission θ with respect to the incident neutron momentum, the observed PFNS, average prompt fission neutron multiplicity, fission cross section, average total kinetic energy TKE, etc. also would be quite dependent on angle θ . Exclusive spectra of $(n, xnf)^{1\dots x}$ neutrons at $\theta \sim 90^\circ$ are consistent with $^{240}\text{Pu}(n, F)$ ($^{239}\text{Pu}(n, F)$, $^{239}\text{Pu}(n, 2n)$) observed cross sections and neutron emission spectra of $^{239}\text{Pu}+n$ interaction at $E_n \lesssim 20$ MeV. The correlations of the angular anisotropy of PFNS with the relative contribution of the (n, n_f) fission chance to the observed fission cross section and angular anisotropy of pre-fission neutron emission are ascertained. The exclusive spectra of $^{240}\text{Pu}(n, xnf)^{1\dots x}$, $^{240}\text{Pu}(n, xn)^{1\dots x}$ and $^{240}\text{Pu}(n, n_f)$ reactions are calculated simultaneously with $^{240}\text{Pu}(n, F)$ and $^{240}\text{Pu}(n, xn)$ cross sections with Hauser-Feshbach formalism, angular anisotropy of $(n, nX)^1$ neutron emission being included. The influence of forward and backward emission of $^{240}\text{Pu}(n, xnf)^{1\dots x}$ pre-fission neutrons on observed PFNS are predicted to be stronger than observed for PFNS of $^{239}\text{Pu}(n, F)$. The ratios of $^{240}\text{Pu}(n, F)$ PFNS average energies $\langle E \rangle$ for forward and backward emission of $^{240}\text{Pu}(n, xnf)^{1\dots x}$ pre-fission neutrons are predicted to be slightly higher than those observed for $^{239}\text{Pu}(n, F)$ PFNS. Calculated PFNS average energies $\langle E \rangle$ are consistent with measured data up to the threshold of $^{240}\text{Pu}(n, 2nf)$ reaction, at higher E_n sloping down of measured data remains unconfirmed.

1. Introduction

Detailed measurement of observed PFNS of $^{240}\text{Pu}(n, F)$ just appeared in [1]. The newest [1] and preliminary data [2–4] on PFNS of $^{240}\text{Pu}(n, F)$ are consistent with the estimates of average energies $\langle E \rangle$ and PFNS shapes [5, 6], though with some exceptions.

The reliability of the modelling of PFNS for neutron-induced fission of ^{239}Pu might be augmented by comparing $^{239}\text{Pu}(n_{th}, f)$ & $^{240}\text{Pu}(sf)$ data sets. Similar augmentation is possible for PFNS of a pair of fission reactions $^{241}\text{Pu}(n_{th}, f)$ & $^{242}\text{Pu}(sf)$. In reaction $^{239}\text{Pu}(n_{th}, f)$ neutrons yield mostly from $J^\pi = 0^+$ states, same as in $^{240}\text{Pu}(sf)$ spontaneous fission neutron spectra (SFNS). Comparison of PFNS of $^{239}\text{Pu}(n_{th}, f)$ and SFNS of $^{240}\text{Pu}(sf)$ [7] in [5, 6] shows that at $\varepsilon < 0.2$ MeV PFNS and SFNS of fissioning nuclide ^{240}Pu depend only weakly on the excitation energy, while at $\varepsilon \gtrsim \langle E \rangle$ the PFNS of $^{239}\text{Pu}(n_{th}, f)$ is much harder than SFNS of $^{240}\text{Pu}(sf)$. The same happens in case of calculated $^{241}\text{Pu}(n_{th}, f)$ PFNS and measured SFNS of $^{242}\text{Pu}(sf)$ [7]. For a pair of reactions $^{240}\text{Pu}(n_{th}, f)$ & $^{241}\text{Pu}(sf)$ such augmentation is hardly would be ever possible, though some guidance stems from comparing a pair of spectra of $^{240}\text{Pu}(n_{th}, f)$ & $^{240}\text{Pu}(sf)$. Some guidance appears also from comparison of calculated $^{240}\text{Pu}(n_{th}, f)$ PFNS and $^{240}\text{Pu}(n, f)$ PFNS data [2, 4] at $E_n \sim 1\text{--}2$ MeV. When the PFNS of $^{240}\text{Pu}(n_{th}, f)$ is eventually fixed, the modelling of PFNS as described in [8, 9] produces acceptable fits [5, 6] of available data on $\langle E \rangle$ and measured $^{240}\text{Pu}(n, f)$ and $^{240}\text{Pu}(n, F)$ PFNS data [2, 3] at $E_n \sim \langle E \rangle$, $E_n \sim E_{nnf}$ and $E_n \sim E_{n2nf}$, here E_{nxf} is the threshold of (n, xnf) reaction. Major parameters of $^{240}\text{Pu}(n_{th}, f)$ PFNS modelling are α , α_1 and E_F^{pre} , they define the kinetic energy of the fragments at the moment of prompt fission neutron emission from the fragments [8, 9]. That may influence $\langle E \rangle$, however, the uncertainty of α value, which leads

¹mvm2386@yandex.ru

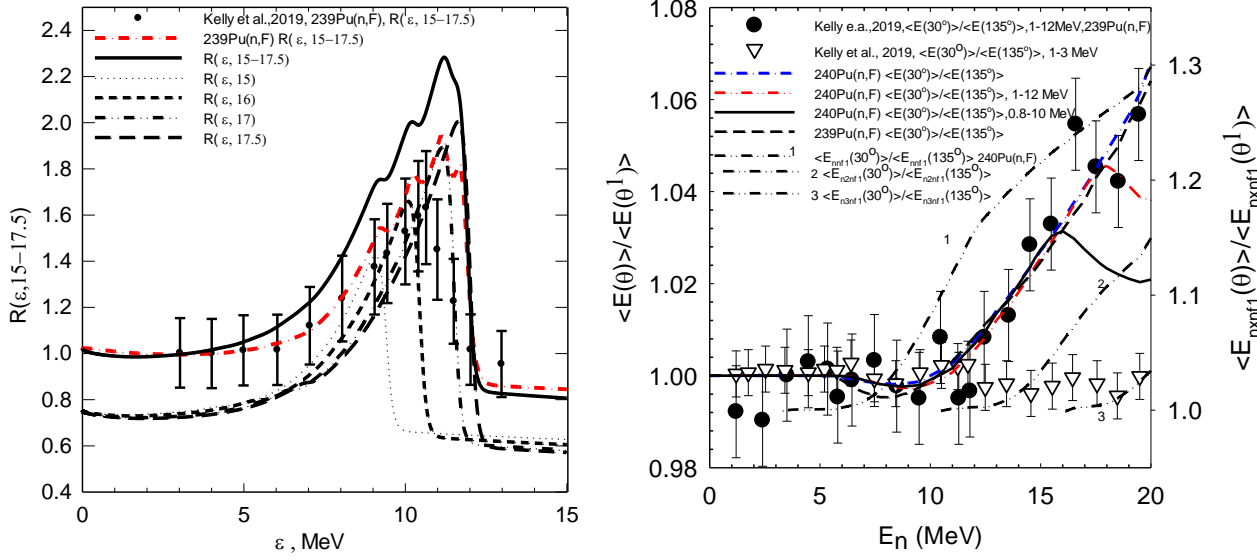


Fig. 1 Ratio $R^{\text{exp}} = S(\varepsilon, E_n \approx 15-17.5, \Delta\theta) / S(\varepsilon, E_n \approx 15-17.5, \Delta\theta^1)$ for $^{239}\text{Pu}(n, F)$ PFNS and calculated ratio $R(\varepsilon, E_n, \Delta\theta, \Delta\theta^1)$ for “forward” ($\Delta\theta \sim 35^\circ-40^\circ$) and “backward” ($\Delta\theta^1 = 130^\circ-140^\circ$) neutron emission. Data points: \bullet – $^{239}\text{Pu}(n, F)$ [17]; full line – $^{240}\text{Pu}(n, F)$ PFNS, equated at $\varepsilon \sim 3-5$ MeV; red dash-dotted line – $^{239}\text{Pu}(n, F)$ PFNS, equated at $\varepsilon \sim 3-5$ MeV; partials of $R(\varepsilon, E_n, \Delta\theta, \Delta\theta^1)$ at $E_n \sim 15-17.5$ MeV for $^{240}\text{Pu}(n, F)$, normalized to unity; $E_n \sim 15$ MeV – dotted line; $E_n \sim 16$ MeV – short dashed line. $E_n \sim 17$ MeV – double dotted dashed line; $E_n \sim 17.5$ MeV – long dashed line.

Fig. 2. PFNS of $^{239}\text{Pu}(n, F)$ and $^{240}\text{Pu}(n, F)$, ratio $\langle E(\theta) \rangle / \langle E(\theta^1) \rangle$. Data points: \blacktriangle – $^{239}\text{Pu}(n, F)$ $\langle E(\theta \approx 30^\circ) \rangle / \langle E(\theta^1 \approx 135^\circ) \rangle$, $\varepsilon \sim 1-12$ MeV [17]; ∇ – $^{239}\text{Pu}(n, F)$, $\langle E(\theta \approx 30^\circ) \rangle / \langle E(\theta^1 \approx 135^\circ) \rangle$, $\varepsilon \sim 1-3$ MeV [17]. Full line – $^{240}\text{Pu}(n, F)$ $\langle E(\theta \approx 30^\circ) \rangle / \langle E(\theta^1 \approx 135^\circ) \rangle$, $\varepsilon \sim 0.8-10$ MeV; blue dash-dotted line – $^{240}\text{Pu}(n, F)$, $\langle E(\theta \approx 30^\circ) \rangle / \langle E(\theta^1 \approx 135^\circ) \rangle$, $\varepsilon \sim 0-20$ MeV; red dash-double dotted line – $^{240}\text{Pu}(n, F)$ $\langle E(\theta \approx 30^\circ) \rangle / \langle E(\theta^1 \approx 135^\circ) \rangle$, $\varepsilon \sim 1-12$ MeV; dashed line – $^{239}\text{Pu}(n, F)$, $\langle E(60^\circ) \rangle / \langle E(90^\circ) \rangle$, $\varepsilon \sim 0-20$ MeV; lines 1, 2, 3 – $^{240}\text{Pu}(n, F)$, $\langle E_{n, \text{xf}}(\theta \approx 30^\circ) \rangle / \langle E_{n, \text{xf}}(\theta^1 \approx 135^\circ) \rangle$, $x = 1, 2, 3$.

to variation of E_F^{pre} values by several MeV or more, changes $\langle E \rangle$ by ~ 0.1 MeV [5, 6]. The analysis of asymmetry of prompt fission neutron emission [5, 6, 9–16] with respect to the incident neutron momentum for $^{239}\text{Pu}(n, F)$ [17–19] and $^{235}\text{U}(n, F)$ [20] reactions, might be applied for prediction of asymmetry of PFNS for $^{240}\text{Pu}(n, F)$ reaction. Angle-averaged data on $^{240}\text{Pu}(n, F)$ PFNS is compatible by the ENDF/B formatted data available at [3] before the paper [1] was published.

Pre-fission neutrons influence the $^{239}\text{Pu}(n, F)$ PFNS shape in the energy range of $E_n \sim E_{\text{nnf}} - 20$ MeV as it was shown in [5, 6]. They influence also the shape of TKE of fission fragments and products [21, 22], prompt fission neutron multiplicity, fission fragment distributions and produce the step-like shape of observed fission cross section. The variation of observed average PFNS energies $\langle E \rangle$ in the vicinity of $^{240}\text{Pu}(n, \text{xf})$ reaction thresholds is stronger than in case of $^{239}\text{Pu}(n, F)$, due to larger contribution of exclusive spectra of $^{240}\text{Pu}(n, \text{xf})^{1 \dots x}$ neutrons (henceforth, the upper indices (1...x) notify the sequence of emitted x pre-fission neutrons. The amplitude of variations of $\langle E \rangle$ in case of $^{240}\text{Pu}(n, F)$ [5, 6] is consistent, up to $^{240}\text{Pu}(n, 2\text{nf})$ reaction threshold, with the preliminary angle-integrated data [2, 3] for $\varepsilon \sim 0.8-10$ MeV energy range.

Pre-fission neutrons in [1–4, 17–20] counted in coincidence with fission fragments, without separation with respect to fragment masses. The pre-fission relatively soft neutrons emitted in a spherically symmetric way relative to the neutron beam momentum. The angular anisotropy of PFNS observed in $^{239}\text{Pu}(n, F)$ [17–19], might be attributed to the pre-equilibrium emission of $^{239}\text{Pu}(n, \text{nf})^1$ neutrons [10]. The direction of

emission of $(n, nX)^1$ neutrons, as well as that of $(n, n\gamma)^1$, $(n, 2n)^1$, $(n, 3n)^1$ and $(n, nf)^1$, $(n, 2nf)^1$ and $(n, 3nf)^1$ neutrons, is correlated with the momentum of the incident neutrons. The direction of the neutrons emitted from the fission fragments correlates with the fission axis direction mostly. Both kinds of neutrons counted in coincidence with fission fragments.

Anisotropy of NES of $^{239}\text{Pu}+n$ interaction observed long ago [23]. The anisotropic contribution of double differential spectra of first neutron, relevant for the excitations of first residual nuclide of 0.5~6 MeV, is evidenced in double differential NES and mostly in the component of $^{239}\text{Pu}(n, n\gamma)^1$ reaction [5, 6, 9, 10]. However, the most investigated to define first neutron spectrum of $(n, nX)^1$ reaction are target nuclides ^{232}Th or ^{238}U , as shown in [13, 24–26]. Neutron emission spectra of $^{238}\text{U}+n$ interaction are strongly anisotropic. The experimental quasi-differential emissive neutron spectra for $^{235}\text{U}+n$, $^{238}\text{U}+n$ and $^{239}\text{Pu}+n$ interactions [27, 28] revealed once again the inadequacy of current NES modelling, envisaged in [11], and stimulated further efforts of NES modelling [29].

The level structures of ^{232}Th , ^{238}U or ^{240}Pu are rather similar, they define the asymmetry of quasi-elastic peak of NES. For example, direct excitation of ^{238}U ground state band levels $J^\pi = 0^+, 2^+, 4^+, 6^+, 8^+$ was accomplished in [26] within rigid rotator model, while that of β -bands of $K^\pi = 0^+$ and γ -bands of $K^\pi = 2^+$, octupole band of $K^\pi = 0^-$ at $U=0\sim 1.2$ MeV was accomplished within soft deformable rotator [24–26]. The net effect of these procedures is the adequate approximation of angular distributions of $^{232}\text{Th}(n, nX)^1$ and $^{238}\text{U}(n, nX)^1$ first neutron inelastic scattering in continuum which corresponds to $U=1.2\sim 6$ MeV excitations for $E_n = 1.2\sim 20$ MeV. The fictitious levels [29], as a substitute for non-pre-equilibrium inelastic scattering, are avoided. That approach is suitable to predict the NES of $^{240}\text{Pu}+n$ interaction.

2. Prompt fission neutron spectra and neutron emission spectra

Prompt fission neutron spectra $S(\varepsilon, E_n, \theta)$ at angle θ relative to the incident neutron beam, is a superposition of exclusive spectra of $(n, xn\text{f})^{1,\dots,x}$ pre-fission neutrons, $-\frac{d^2\sigma_{n\text{xn}}^k(\varepsilon, E_n, \theta)}{d\varepsilon d\theta}$ ($x=1, 2, 3; k=1, \dots, x$), and spectra of prompt fission neutrons, emitted by fission fragments, $S_{A+1-x}(\varepsilon, E_n, \theta)$:

$$\begin{aligned}
S(\varepsilon, E_n, \theta) &= \tilde{S}_{A+1}(\varepsilon, E_n, \theta) + \tilde{S}_A(\varepsilon, E_n, \theta) + \tilde{S}_{A-1}(\varepsilon, E_n, \theta) + \tilde{S}_{A-2}(\varepsilon, E_n, \theta) = \\
&v_p^{-1}(E_n, \theta) \cdot \{ v_{p1}(E_n) \cdot \beta_1(E_n, \theta) S_{A+1}(\varepsilon, E_n, \theta) + v_{p2}(E_n - \langle E_{n\text{nf}}(\theta) \rangle) \beta_2(E_n, \theta) S_A(\varepsilon, E_n, \theta) + \\
&+ \beta_2(E_n, \theta) \frac{d^2\sigma_{n\text{nf}}^1(\varepsilon, E_n, \theta)}{d\varepsilon d\theta} + v_{p3}(E_n - B_n^A - \langle E_{n2\text{nf}}^1(\theta) \rangle - \langle E_{n2\text{nf}}^2(\theta) \rangle) \beta_3(E_n, \theta) S_{A-1}(\varepsilon, E_n, \theta) + \beta_3(E_n, \theta) \times \\
&\left[\frac{d^2\sigma_{n2\text{nf}}^1(\varepsilon, E_n, \theta)}{d\varepsilon d\theta} + \frac{d^2\sigma_{n2\text{nf}}^2(\varepsilon, E_n, \theta)}{d\varepsilon d\theta} \right] + v_{p4}(E_n - B_n^A - B_n^{A-1} - \langle E_{n3\text{nf}}^1(\theta) \rangle - \langle E_{n3\text{nf}}^2(\theta) \rangle - \langle E_{n3\text{nf}}^3(\theta) \rangle) \times \\
&\beta_4(E_n, \theta) S_{A-2}(\varepsilon, E_n, \theta) + \beta_4(E_n, \theta) \left[\frac{d^2\sigma_{n3\text{nf}}^1(\varepsilon, E_n, \theta)}{d\varepsilon d\theta} + \frac{d^2\sigma_{n3\text{nf}}^2(\varepsilon, E_n, \theta)}{d\varepsilon d\theta} + \frac{d^2\sigma_{n2\text{nf}}^3(\varepsilon, E_n, \theta)}{d\varepsilon d\theta} \right] \}. \quad (1)
\end{aligned}$$

In equation (1) $\tilde{S}_{A+1-x}(\varepsilon, E_n, \theta)$ is the contribution of x -chance fission to the observed PFNS $S(\varepsilon, E_n, \theta)$, $\langle E_{n\text{xn}}^k(\theta) \rangle$ – average energy of k -th neutron of $(n, xn\text{f})$ reaction with exclusive neutron spectrum

$\frac{d^2\sigma_{n\text{xn}}^k(\varepsilon, E_n, \theta)}{d\varepsilon d\theta}$, $k \leq x$. Spectra $S(\varepsilon, E_n, \theta)$, $S_{A+1-x}(\varepsilon, E_n, \theta)$ and $\frac{d^2\sigma_{n\text{xn}}^k(\varepsilon, E_n, \theta)}{d\varepsilon d\theta}$ are normalized to unity. Index x denotes the fission chance of $^{241-x}\text{Pu}$ nuclides after emission of x pre-fission neutrons, $\beta_x(E_n, \theta) = \sigma_{n, xn\text{f}}(E_n, \theta) / \sigma_{n, F}(E_n, \theta)$ – relative contribution of x -th fission chance to the observed fission cross section $\sigma_{n, F}(E_n, \theta)$, $v_p(E_n, \theta)$ is the average number of prompt fission neutrons, $v_{px}(E_n)$ – average number of prompt fission neutrons, emitted by the fragments of fission of $^{241-x}\text{Pu}$ nuclides. Spectra of prompt

fission neutrons, emitted from fragments, $S_{A+1-x}(\varepsilon, E_n, \theta)$, as proposed in [8], were approximated by the sum of two Watt [30] distributions with different temperatures, the temperature of the light fragment being higher.

Modelling the angular distribution for the exclusive spectra of pre-fission neutrons $^{239}\text{Pu}(n, xnf)^{1, \dots, x}$ [10], we reproduced PFNS ratios $R(\varepsilon, E_n, \Delta\theta, \Delta\theta^1) = \langle S(\varepsilon, E_n, \Delta\theta) \rangle_{\Delta E_n} / \langle S(\varepsilon, E_n, \Delta\theta^1) \rangle_{\Delta E_n}$ in angular ranges $\Delta\theta \sim 35^\circ - 40^\circ$ and $\Delta\theta^1 \approx 130^\circ - 140^\circ$ for wide energy range of $\Delta E_n \sim 15 - 17.5$ MeV. These ratios were extracted from measured data, shown on Fig.3 of paper [17], The ratios $R(\varepsilon, \Delta E_n, \Delta\theta, \Delta\theta^1)$ shown on Fig. 1. Alternative representation of PFNS, against that shown on Fig.3 in paper [17], as a ratio $R^{\text{exp}} = S(\varepsilon, E_n \approx 15 - 17.5, \Delta\theta) / S(\varepsilon, E_n \approx 15 - 17.5, \Delta\theta^1)$ for $\Delta\theta \sim 35^\circ - 40^\circ$ (forward direction) and $\Delta\theta^1 = 130^\circ - 140^\circ$ (backward direction) is virtually independent upon the normalizations adopted in [17]. In [11, 13] it was shown, that the calculated ratios $R(\varepsilon, E_n, \Delta\theta, \Delta\theta^1)$ for $^{232}\text{Th}(n, F)$ and $^{238}\text{U}(n, F)$ strongly depend on $^{232}\text{Th}(n, xnf)^{1, \dots, x}$ and $^{238}\text{U}(n, xnf)^{1, \dots, x}$ reactions relative contributions to the respective observed PFNS and fission cross sections as well. Anomalous values of $R(\varepsilon, E_n, \Delta\theta, \Delta\theta^1)$ were predicted for the $^{232}\text{Th}(n, F)$ reaction [13]. Blind application of approach, described in [9–16], to predict angle-integrated PFNS of $^{240}\text{Pu}(n, F)$ [5], and then the asymmetry of pre-fission neutrons [5, 6], produces curves of $R(\varepsilon, E_n, \Delta\theta, \Delta\theta^1)$ for $^{240}\text{Pu}(n, F)$, shown on Fig. 1.

The ratios of average energies of PFNS $\langle E(\theta \approx 37.5^\circ) \rangle / \langle E(\theta^1 \approx 135^\circ) \rangle$, i.e. of energies $\langle E \rangle$ for neutrons counted at angular intervals $\Delta\theta \sim 35^\circ - 40^\circ$ and $\Delta\theta^1 \sim 130^\circ - 150^\circ$ in $E_n \sim 1 - 20$ MeV incident neutron energy range were reproduced for $^{239}\text{Pu}(n, F)$ and predicted for $^{240}\text{Pu}(n, F)$ also (Fig. 2). The main factor for the observed features of PFNS, like ratios $R(\varepsilon, E_n, \Delta\theta, \Delta\theta^1)$ and $\langle E(\theta \approx 37.5^\circ) \rangle / \langle E(\theta^1 \approx 135^\circ) \rangle$, is the excitation energy of fissioning Pu nuclides emerging after x pre-fission neutron emission. Average energies for the angle-integrated PFNS of $^{240}\text{Pu}(n, F)$ for $\varepsilon \sim 0.8 - 10$ MeV [2, 3] are compared with calculations, described in [5, 6], on Fig. 3. Correlation of the $\langle E_{n_{nf}}^1(\theta) \rangle$ – average energy of 1st neutron of (n, nf) reaction with $\langle E \rangle$ of PFNS is evident. At higher incident energies the influence of $\langle E_{n_{2nf}}^{1,2}(\theta) \rangle$ – average energies of 1st and 2nd neutrons of $^{240}\text{Pu}(n, 2nf)$ reaction is smaller, than observed in [1, 2, 3].

Since the energy and angular intervals in measurements of [17] rather wide, number of detected prompt fission neutrons one should estimate in similar fashion as in NES. Double differential NES defined as

$$\begin{aligned} \frac{d^2\sigma(\varepsilon, E_n, \theta)}{d\varepsilon d\theta} &= \frac{1}{2\pi} \left[v_p(E_n, \theta) \sigma_{nF}(E_n, \theta) S(\varepsilon, E_n, \theta) + \sigma_{n\gamma}(\varepsilon, E_n, \theta) \frac{d^2\sigma_{n\gamma}^1(\varepsilon, E_n, \theta)}{d\varepsilon d\theta} + \right. \\ &\sigma_{n2n}(\varepsilon, E_n, \theta) \left(\frac{d^2\sigma_{n2n}^1(\varepsilon, E_n, \theta)}{d\varepsilon d\theta} + \frac{d^2\sigma_{n2n}^2(\varepsilon, E_n, \theta)}{d\varepsilon d\theta} \right) + \\ &\left. \sigma_{n3n}(\varepsilon, E_n, \theta) \left(\frac{d^2\sigma_{n3n}^1(\varepsilon, E_n, \theta)}{d\varepsilon d\theta} + \frac{d^2\sigma_{n3n}^2(\varepsilon, E_n, \theta)}{d\varepsilon d\theta} + \frac{d^2\sigma_{n3n}^3(\varepsilon, E_n, \theta)}{d\varepsilon d\theta} \right) + \right. \\ &\left. \sum_q \frac{d\sigma_{n\gamma}(\varepsilon, E_q, E_n, \theta)}{d\theta} G(\varepsilon, E_q, E_n, \Delta\theta) \right], \end{aligned} \quad (2)$$

$$G(\varepsilon, E_q, E_n, \Delta\theta) = \frac{2}{\Delta\theta \sqrt{\pi}} \exp \left\{ - \left[\frac{\varepsilon - (E_n - E_q)}{\Delta\theta} \right]^2 \right\}. \quad (3)$$

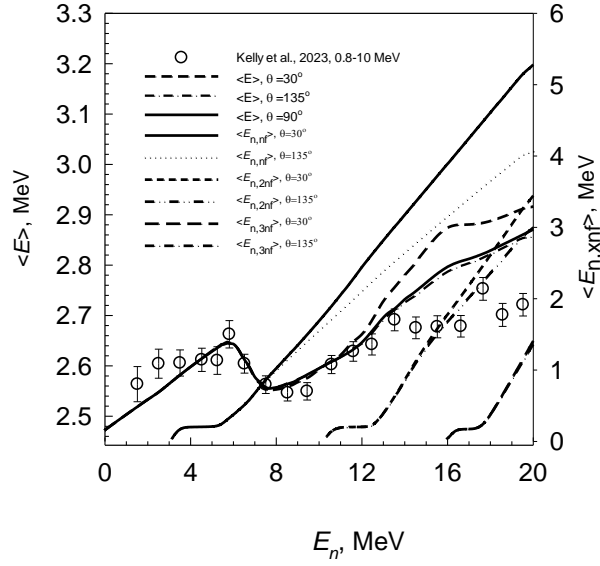


Fig. 3 PFNS $\langle E \rangle$ for $^{240}\text{Pu}(n, F)$, $\varepsilon \sim 0.8\text{--}10$ MeV: \circ —[2, 3]; full line, $-\langle E(90^\circ) \rangle$; dashed line $-\langle E(30^\circ) \rangle$; dash-dotted line $-\langle E(135^\circ) \rangle$; solid line $-\langle E_{n,nf}(\theta \approx 30^\circ) \rangle$; dotted line $-\langle E_{n,nf}(\theta \approx 135^\circ) \rangle$; dashed line $-\langle E_{n,2nf}(\theta \approx 30^\circ) \rangle$; dashed — double dotted line $-\langle E_{n,2nf}(\theta \approx 135^\circ) \rangle$; long dashed line $-\langle E_{n,3nf}(\theta \approx 30^\circ) \rangle$; dash dotted line $-\langle E_{n,3nf}(\theta \approx 135^\circ) \rangle$.

NES in Eq. (2) is a superposition of prompt fission neutron spectra $S(\varepsilon, E_n, \theta)$, exclusive neutron spectra of

$(n, n\gamma)^1$, $(n, 2n)^{1,2}$ and $(n, 3n)^{1,2,3}$ reactions, $\frac{d^2\sigma_{n,xf}^k(\varepsilon, E_n, \theta)}{d\varepsilon d\theta}$, normalized to unity, and spectra of elastic and

inelastic scattered neutrons, followed by excitation of collective levels E_q of ^{240}Pu nuclide, $\frac{d^2\sigma_{nny}(\varepsilon, E_q, E_n, \theta)}{d\varepsilon d\theta}$

. $G(\varepsilon, E_q, E_n, \Delta_\theta)$ —resolution function, which depends on E_n and may weakly depend on θ and E_q . The calculated NES are normalized using average prompt fission neutron multiplicity, (n, F) and (n, xn) cross sections.

The part of anisotropic double differential spectrum of first neutron relevant for the excitations close to the fission barrier value of ^{240}Pu nuclide (corresponds to second chance fission reaction), will be pronounced in exclusive spectra of $(n, nf)^1$, $(n, 2nf)^1$ and $(n, 2n)^1$ at $E_n \gtrsim 12$ MeV, at various pre-fission neutron emission angles θ . Angular distribution of pre-fission neutrons in [17] was extracted from the observed PFNS of $^{239}\text{Pu}(n, F)$ by subtracting the post-fission neutron spectrum, which was estimated in rather approximate manner, due to adopted normalizations to equal number of fission events for any angle θ .

3. Fission cross section $\sigma_{n,F}(E_n)$ and prompt neutron multiplicity $\nu_p(E_n)$

Contributions $\beta_x(E_n, \theta)$ of x -th fission chance (n, xnf) to the observed fission cross section $\sigma(n, F)$ in Eq.(1) and Eq.(2) is about the main factor influencing the shape of PFNS. Figure 4 shows the values $\beta_1(E_n)$ and $\beta_2(E_n)$ of 1st and 2nd fission chances to the observed fission cross sections $\sigma(n, F)$ of $^{239}\text{Pu}(n, F)$ and $^{240}\text{Pu}(n, F)$ reactions. Contributions $\beta_1 = \sigma_{n,f} / \sigma_{n,F}$ and $\beta_2 = \sigma_{n,nf} / \sigma_{n,F}$ of [31] were estimated by the analysis of prompt fission neutron multiplicity distributions. They are quite different from $\beta_x(E_n)$ values, used in [5, 6, 9–16]. The $\beta_x(E_n)$ estimate of [31] seems to be rather unstable with respect to the experimental uncertainties. The experimental points $\beta_x(E_n)$ (Fig. 4) were obtained

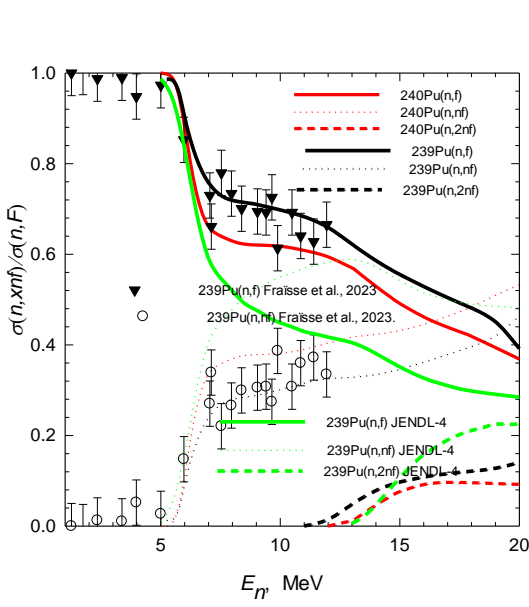


Fig.4. Ratios of partial components (n,xnf) to the observed fission cross section $^{239,240}\text{Pu}(n, F)$ and $^{239,240}\text{Pu}(n, F)$. Red curves — $^{240}\text{Pu}(n,xnf)$; black curves — $^{239}\text{Pu}(n,xnf)$; green curves — $^{240}\text{Pu}(n,xnf)$ of [32]; \circ — [31]; \blacktriangledown — [31].

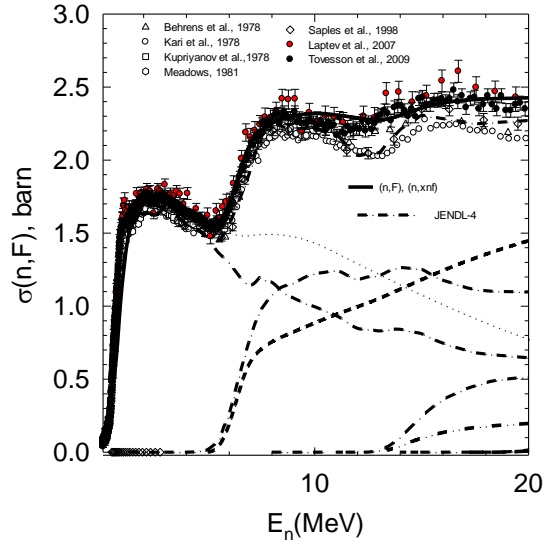


Fig.5. Partial $^{240}\text{Pu}(n,xnf)$ components of $^{240}\text{Pu}(n, F)$; \circ — [33]; \diamond — [34]; \circ — [35]; \square — [36]; Δ — [37]; \bullet — [38]; \bullet — [39]; solid line — $^{240}\text{Pu}(n, F)$; dotted line — $^{240}\text{Pu}(n, f)$; dashed line — $^{240}\text{Pu}(n, nf)$; dashed double dotted line — $^{240}\text{Pu}(n, 2nf)$; ; ; dash dotted curves — $^{240}\text{Pu}(n,xnf)$ of [32];

renormalizing data of [31] as $\tilde{\beta}_2(E_n) = 0.7\beta_2(E_n)$. When renormalized, $\tilde{\beta}_1(E_n)$ and $\tilde{\beta}_2(E_n)$ appear quite consistent with those used in [5, 6, 9–16], especially near reaction thresholds of $^{239}\text{Pu}(n,xnf)$ reaction. Estimates of $\beta_1(E_n)$ and $\beta_2(E_n)$ of $^{239}\text{Pu}(n, F)$ in [9] have much more grounds, since it allows reproduce available observed PFNS at $E_{n,f} \lesssim E_n \lesssim 20$ MeV using $\tilde{S}_{240}(\varepsilon, E_n)$, $\tilde{S}_{239}(\varepsilon, E_n)$ and $\tilde{S}_{238}(\varepsilon, E_n)$ contributions of $^{239}\text{Pu}(n,xnf)$ reactions. Values of $\beta_2(E_n)$ for $^{240}\text{Pu}(n, F)$ are systematically higher than $\beta_2(E_n)$ of $^{239}\text{Pu}(n, F)$, the $\beta_2(E_n)$ for $^{240}\text{Pu}(n, F)$ are incompatible with relevant estimate of [32].

The observed fission cross section of $^{240}\text{Pu}(n, F)$ was calculated as

$$\sigma_{nF}(E_n) = \sigma_{nf}(E_n) + \sum_{x=1}^X \sigma_{n,xnf}(E_n), \quad (4)$$

and compared with measured data [33–39] on Fig. 5. The (n,xnf) reaction contributions are defined by the fission probability $P_{f(241-x)}^{1\pi}(E)$ of $^{241-x}\text{Pu}$ nuclides:

$$\sigma_{n,xnf}(E_n) = \sum_{J\pi} \int_0^{U_x} W_{A+1-x}^{J\pi}(U) P_{f(A+1-x)}^{J\pi}(U) dU, \quad (5)$$

here $W_{A+1-x}^{J\pi}(U)$ is the population of excited states of $^{241-x}\text{Pu}$ nuclides with excitation energy U , after emission of x pre-fission neutrons. Calculated cross sections of $^{240}\text{Pu}(n,xnf)$ reactions are much different from estimates of [32] (see Fig. 5). If the latter estimates of $^{240}\text{Pu}(n,xnf)$ contributions would be used for calculation of PFNS,

the discrepancies with present calculations would be due to differing contribution of $^{240}\text{Pu}(n, nf)^1$ and $^{240}\text{Pu}(n, 2nf)^{1,2}$ pre-fission neutrons and neutrons emitted from the fragments $S_{241-x}(\varepsilon, E_n, \theta)$.

Observed average number of prompt fission neutrons $\nu_p(E_n)$ defined as superposition of pre-fission neutrons and neutrons, coming from the fission fragments of $^{241-x}\text{Pu}$ nuclides, cooled down by the pre-fission neutron emission is

$$\nu_p(E_n) = \nu_{post} + \nu_{pre} = \sum_{x=1}^X \nu_{px}(E_{nx}) + \sum_{x=1}^X (x-1) \cdot \beta_x(E_n). \quad (6)$$

The post-fission, $\nu_{post}(E_n)$ and pre-fission $\nu_{pre}(E_n)$, as well as (n, xnf) partial contributions of $\nu_p(E_n)$ were obtained via consistent description of $\nu_p(E_n)$ and observed fission cross sections at $E_n < 20$ MeV (see Fig. 6).

Average prompt fission neutron number $\nu_p(E_n)$ of $^{240}\text{Pu}(n, F)$ was measured in [40–42]. Partial average neutron multiplicities $\nu_{px}(E_{nx})$ define relative contributions of pre-fission neutrons with spectra $d\sigma_{nxf}^k/d\varepsilon$ and prompt neutrons, emitted from fission fragments, with spectra $S_{A+1-x}(\varepsilon, E_n)$, see Eq. (2) and equations for $\tilde{S}_{A+1-x}(\varepsilon, E_n)$. To calculate $\nu_p(E_n)$ when $E_n > E_{nxf}$, the data on $\nu_p(E_n)$ for $^{241-x}\text{Pu}(n, F)$ at $E_n < E_{nxf}$ should be used, when available. The partial contributions $\tilde{S}_{A+1-x}(\varepsilon, E_n)$ to the PFNS correlate with partial contributions $\nu_{px}(E_{nx})$ to $\nu_p(E_n)$. Figure 6 compares the model calculation of $\nu_p(E_n)$ (Eq. (6)) with measured data. Partial contributions of $^{240}\text{Pu}(n, F)$, $^{240}\text{Pu}(n, nf)$ and $^{240}\text{Pu}(n, 2nf)$ reactions are shown, as well as lumped contributions of six pre-fission neutrons of $^{240}\text{Pu}(n, nf)^1$, $^{240}\text{Pu}(n, 2nf)^{1,2}$ and $^{240}\text{Pu}(n, 3nf)^{1,2,3}$ reactions, $\nu_{pre}(E_n)$, and post-fission neutrons, emitted from relevant fission fragments, $\nu_{post}(E_n)$. Partial contribution of $^{240}\text{Pu}(n, nf)$ reaction influences but still only weakly smooth energy dependence of $\nu_p(E_n)$ around E_{nxf} reaction threshold. The strong bump may appear in $\sigma_{n,F}(E_n)$ and $\nu_p(E_n)$ of $^{232}\text{Th}(n, F)$ or $^{230}\text{Th}(n, F)$, when $E_n > E_{nxf}$ [43, 44]. That happens because of net influence of wide (~ 1.5 MeV) pairing gap at saddle deformations, relatively high fission barrier of ^{232}Th or ^{230}Th nuclides and rather high thresholds of $^{232}\text{Th}(n, 2n)$ or $^{230}\text{Th}(n, 2n)$ reactions. In case of $^{238}\text{U}(n, F)$ or $^{240}\text{Pu}(n, F)$ only small steps are observed in $\sigma_{n,F}(E_n)$ [43, 45]. The values of $\nu_{post}(E_n)$ and $\nu_{pre}(E_n)$ of $^{240}\text{Pu}(n, F)$ and $^{239}\text{Pu}(n, F)$ [9] are influenced by values $\beta_x(E_n) = \sigma_{n,xnf} / \sigma_{n,F}$ mostly (see Fig. 6).

4. Exclusive pre-fission neutron spectra $d^2\sigma_{nxf}^k/d\varepsilon d\theta$

To calculate contributions of pre-fission neutrons with spectra $d^2\sigma_{nxf}^k/d\varepsilon d\theta$ to the PFNS $S(\varepsilon, E_n, \theta)$ (Eq. 1) the neutron emission spectrum of $(n, nX)^1$ reaction, $\frac{d^2\sigma_{nX}^1(\varepsilon, E_n, \theta)}{d\varepsilon d\theta}$, should be defined. It is the sum of compound and weakly dependent on emission angle pre-equilibrium components, the procedure followed for years. To reproduce angular asymmetry of NES a phenomenological function was proposed in [9, 10], modelling energy and angle dependence of NES due to first neutron inelastic scattering in continuum [9–16]:

$$\frac{d^2\sigma_{nnX}^1(\varepsilon, E_n, \theta)}{d\varepsilon d\theta} \approx \frac{d^2\tilde{\sigma}_{nnX}^1(\varepsilon, E_n, \theta)}{d\varepsilon d\theta} + \sqrt{\frac{\varepsilon}{E_n}} \frac{\omega(\theta)}{E_n - \varepsilon} \quad (7)$$

$$\omega(\theta) = 0.4 \cos^3(\theta) + 0.16 \quad (8)$$

Angle-averaged function $\omega(\theta)$ [9—16], $\langle \omega(\theta) \rangle_\theta$ for angles $\theta_2 - \theta_1 = 135^\circ - 30^\circ$ [17], is approximated as $\langle \omega(\theta) \rangle_\theta \approx \omega(90^\circ)$, then angle-integrated spectrum is

$$\frac{d\sigma_{nnX}^1(\varepsilon, E_n)}{d\varepsilon} \approx \frac{d\tilde{\sigma}_{nnX}^1(\varepsilon, E_n)}{d\varepsilon} + \sqrt{\frac{\varepsilon}{E_n}} \frac{\langle \omega(\theta) \rangle_\theta}{E_n - \varepsilon} \cdot \quad (9)$$

To retain the flux conservation in cross section and spectra calculations the compound reaction cross sections renormalized to account for extra semi-direct neutron emission:

$$\sigma_c(E_n) = \sigma_a(E_n)(1 - q - \tilde{q}) \quad (10)$$

Emission spectrum of $(n, nX)^1$, q -ratio of pre-equilibrium neutrons in a standard pre-equilibrium model [46],

$$\frac{d\tilde{\sigma}_{nnX}^1(\varepsilon, E_n)}{d\varepsilon} = \sum_{J, \pi} W_{240}^{J\pi}(E_n - \varepsilon, \theta), \quad (11)$$

depends on fission probability of ^{241}Pu nuclide, $W_{240}^{J\pi}(E_n - \varepsilon, \theta)$ is the population of residual nuclide ^{240}Pu states with spin/parity J^π and excitation energy $U = E_n - \varepsilon$, after first neutron emission at angle θ . It defines the exclusive spectra of each partial reaction, $d\sigma_{nxf}^k/d\varepsilon$ or $d\sigma_{nX}^k/d\varepsilon$, as well as $d^2\sigma_{nxf}^k/d\varepsilon d\theta$ or $d^2\sigma_{nX}^k/d\varepsilon d\theta$ in STAPRE code framework [46]. Henceforth the indexes J^π in fission, Γ_f , neutron Γ_n and total Γ widths described in [45], as well as relevant summations, omitted. The angular dependence of partial width, calculated with spin and parity conservation, is due to dependence of excitation energy of residual nuclides on the emission angle θ of first neutron. The exclusive spectra of pre-fission $(n, nf)^1$ neutrons are

$$\frac{d^2\sigma_{nnf}^1(\varepsilon, E_n, \theta)}{d\varepsilon d\theta} = \frac{d^2\sigma_{nnX}^1(\varepsilon, E_n, \theta)}{d\varepsilon d\theta} \frac{\Gamma_f^{240}(E_n - \varepsilon, \theta)}{\Gamma^{240}(E_n - \varepsilon, \theta)}. \quad (12)$$

First neutron spectra for reaction $(n, 2nf)$, $(n, 2nf)^1$, is defined as:

$$\frac{d^2\sigma_{n2nf}^1(\varepsilon, E_n, \theta)}{d\varepsilon d\theta} = \int_0^{E - B_n^{240}} \frac{d^2\sigma_{n2nX}^1(\varepsilon, E_n, \theta)}{d\varepsilon d\theta} \frac{\Gamma_f^{239}(E_n - B_n^{240} - \varepsilon - \varepsilon_1)}{\Gamma^{239}(E_n - B_n^{240} - \varepsilon - \varepsilon_1)} d\varepsilon_1, \quad (13)$$

here first neutron spectra of $(n, 2nX)$ reaction, $(n, 2nX)^1$, is defined by the neutron spectrum of $(n, nX)^1$ and neutron emission probability of nuclide ^{240}Pu as:

$$\frac{d^2\sigma_{n2nX}^1(\varepsilon, E_n, \theta)}{d\varepsilon d\theta} = \frac{d^2\sigma_{nnX}^1(\varepsilon, E_n, \theta)}{d\varepsilon d\theta} \frac{\Gamma_n^{240}(E_n - \varepsilon, \theta)}{\Gamma^{240}(E_n - \varepsilon, \theta)}. \quad (14)$$

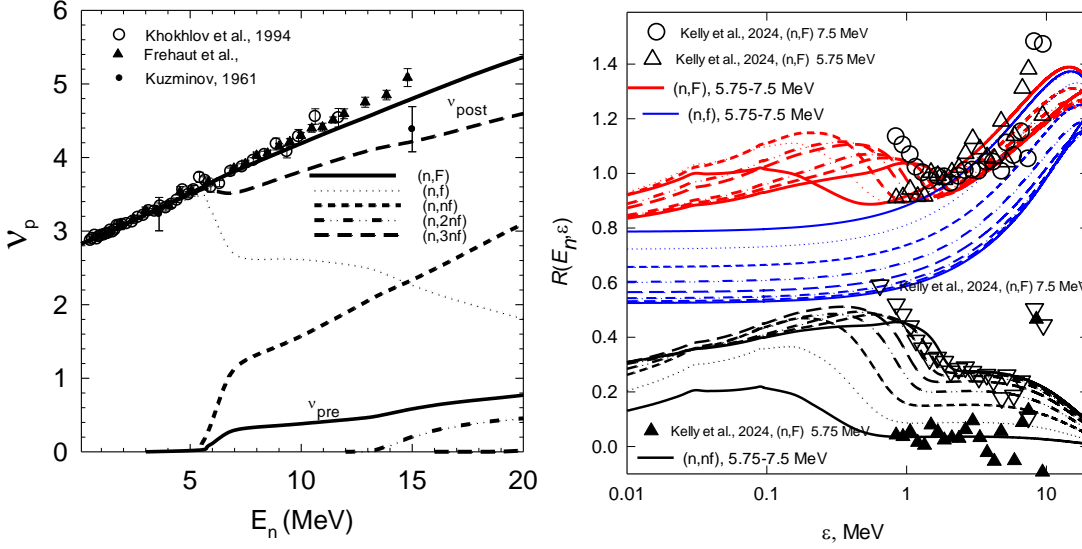


Fig. 6. Average number of prompt fission neutrons of $^{240}\text{Pu}(n,F)$ and its partial components: solid line — ^{240}Pu ; dotted line — $^{240}\text{Pu}(n, f)$; dashed line — $^{240}\text{Pu}(n, nf)$; dashed double dotted line — $^{240}\text{Pu}(n, 2nf)$; dashed line — V_{post} ; solid line — V_{pre} ; \circ — [40]; \blacktriangle — [41]; \bullet — [42].

Fig. 7. PFNS of $^{240}\text{Pu}(n,F)$ at $E_n \sim 5.75 - 7.5$ MeV with step of 0.25 MeV and its partial components: red lines — $^{240}\text{Pu}(n, F)$; blue lines — $^{240}\text{Pu}(n, f)$; black lines — $^{240}\text{Pu}(n, nf)$; \circ — $^{240}\text{Pu}(n, F)$ [1], 7.5 MeV; ∇ — $^{240}\text{Pu}(n, nf)$ [1], 7.5 MeV; Δ — $^{240}\text{Pu}(n, F)$ [1], 5.75 MeV; \blacktriangle — $^{240}\text{Pu}(n, nf)$ [1], 5.75 MeV.

Phenomenological approach of Eqs. (2)–(14) enables to reproduce angular dependent NES in case of $^{232}\text{Th}+n$, $^{235}\text{U}+n$, $^{238}\text{U}+n$ and $^{239}\text{Pu}+n$ interactions [9–16]. Angle-integrated exclusive spectra of pre-fission $^{240}\text{Pu}(n,nf)^1$ neutrons are represented as

$$\frac{d\sigma_{nnf}^1(\varepsilon, E_n)}{d\varepsilon} = \frac{d\sigma_{nnX}^1(\varepsilon, E_n, \theta)}{d\varepsilon} \frac{\Gamma_f^{240}(E_n - \varepsilon)}{\Gamma^{240}(E_n - \varepsilon)}. \quad (15)$$

Figure 7 shows the PFNS and interplay of pre-fission neutrons and prompt fission neutrons of $^{240}\text{Pu}(n,nf)$ in the incident neutron energy range $E_n \sim 5.75 - 7.5$ MeV with a step of $E_n \sim 0.25$ MeV. Preliminary PFNS data of [2, 3] in the energy range $E_n \sim 7 - 8$ MeV and calculated PFNS at $E_n \sim 7.5$ MeV [5, 6, 9] are consistent with each other. However, it seems the cut-off energy E_{nnf1} of pre-fission $^{240}\text{Pu}(n,nf)^1$ neutrons [2, 3] is shifted to higher energies ε in comparison with calculations of [5, 6, 9].

PFNS, calculated at $E_n \sim 5.75 - 7.5$ MeV demonstrate how the pre-fission neutrons influence the PFNS shapes. In fact, $\langle E \rangle$ attains the value observed at $E_n \sim 5$ MeV only at $E_n \sim 12$ MeV (see Fig. 3). The data of [1] at $E_n \sim 5.5 - 6.0$ MeV and $E_n \sim 7.0 - 8.0$ MeV reveal the influence of pre-fission $^{240}\text{Pu}(n,nf)^1$ neutrons on the PFNS shape at $\varepsilon \gtrsim E_{nnf1}$. Due to cooling down of nuclides ^{240}Pu in the reaction $^{240}\text{Pu}(n,nf)$ the PFNS at $E_n \sim 5.75$ MeV increases more steeply than that at $E_n \sim 7.5$ MeV. The comparison of calculated $^{240}\text{Pu}(n,nf)$ reaction contribution with the quasi-experimental data [1], obtained by subtracting the calculated $^{240}\text{Pu}(n,f)$ contribution at $E_n \sim 7.5$ MeV from PFNS data of [1] shows good consistency of shapes both at $\varepsilon \lesssim E_{nnf1}$ and $\varepsilon \gtrsim E_{nnf1}$. At $E_n \sim 5.75$ MeV the pre-fission neutrons are not observed, but they influence the PFNS contribution $S_A(\varepsilon, E_n, \theta)$ of the second chance fission due to cooling down of nuclides ^{240}Pu in the reaction $^{240}\text{Pu}(n,nf)$. The comparison of calculated $^{240}\text{Pu}(n,nf)$ reaction contribution with the quasi-experimental data [1], obtained by subtracting the calculated $^{240}\text{Pu}(n,f)$ contribution at $E_n \sim 5.75$ MeV from PFNS data of [1] shows good consistency of shapes at $\varepsilon \gtrsim E_{nnf1}$.

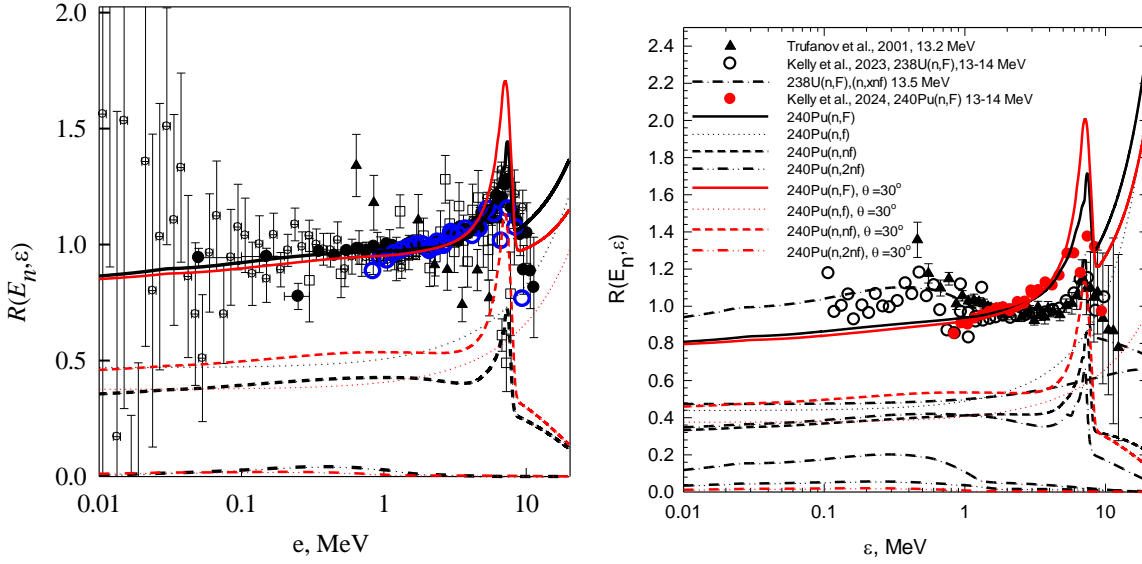


Fig.8. Ratios of partial components of PFNS of $^{240}\text{Pu}(n, F)$ at $E_n = 13.5$ MeV relative to Maxwellian type distribution with $T = 1.4241$ MeV: — — $^{240}\text{Pu}(n, F)$; ••• — $^{240}\text{Pu}(n, F)$; - - - $^{240}\text{Pu}(n, nf)$; - - • - - $^{240}\text{Pu}(n, 2nf)$; — — $^{240}\text{Pu}(n, F), \theta = 30^\circ$; ••• — $^{240}\text{Pu}(n, F), \theta = 30^\circ$; - - - $^{240}\text{Pu}(n, nf), \theta = 30^\circ$; - - • - - $^{240}\text{Pu}(n, 2nf), \theta = 30^\circ$; ○ — $^{239}\text{Pu}(n, F)$ [18]; ● — $^{239}\text{Pu}(n, F)$ [19]; □ — $^{239}\text{Pu}(n, F)$ [47]; ▲ — $^{239}\text{Pu}(n, F)$ [48]; ○ — $^{240}\text{Pu}(n, F)$ [1].

Fig.9. Ratios of partial components of PFNS of $^{240}\text{Pu}(n, F)$ at $E_n = 13.5$ MeV relative to Maxwellian type distribution with $T = 1.4241$ MeV: ● — $^{240}\text{Pu}(n, F)$ [1]; — — $^{240}\text{Pu}(n, F)$; ••• — $^{240}\text{Pu}(n, F)$; - - - $^{240}\text{Pu}(n, nf)$; - - • - - $^{240}\text{Pu}(n, 2nf)$; — — $^{240}\text{Pu}(n, F), \theta = 30^\circ$; ••• — $^{240}\text{Pu}(n, F), \theta = 30^\circ$; - - - $^{240}\text{Pu}(n, nf), \theta = 30^\circ$; - - • - - $^{240}\text{Pu}(n, 2nf), \theta = 30^\circ$; ○ — $^{239}\text{Pu}(n, F)$ [18]; ▲ — $^{238}\text{U}(n, F)$ [49]; ○ — $^{238}\text{U}(n, F)$ [50]; - • - $^{238}\text{U}(n, F), ^{238}\text{U}(n, nf)$.

5. Angular distribution of $^{239}\text{Pu}(n, xnf)$ pre-fission neutrons

Exclusive pre-fission neutron spectra of $^{240}\text{Pu}(n, nf)^1$ comprise small part of $(n, nX)^1$ spectrum, nonetheless it might be argued that they are responsible for angular dependence of PFNS with respect to the incident neutron beam [10]. Figure 8 shows the partial contributions of $^{240}\text{Pu}(n, f)$, $^{240}\text{Pu}(n, nf)$ and $^{240}\text{Pu}(n, 2nf)$ contributions to $^{240}\text{Pu}(n, F)$ PFNS at $E_n \sim 13.5$ MeV at $\theta \sim 90^\circ$ and $\theta \sim 30^\circ$. Even at this low incident energy PFNS shape for forward emission is much harder than that corresponding to pre-fission neutron emission at $\theta \sim 30^\circ$. The hardening of $\langle E \rangle$ at $\theta \sim 30^\circ$ is due to increase of second chance fission contribution

and hardening of $\frac{d^2 \sigma_{nnf}^1(\varepsilon, E_n, \theta)}{d\varepsilon d\theta}$. Figure 9 compares the partial contributions of $^{240}\text{Pu}(n, f)$, $^{240}\text{Pu}(n, nf)$ and $^{240}\text{Pu}(n, 2nf)$ contributions to $^{240}\text{Pu}(n, F)$ PFNS at $E_n \sim 13.5$ MeV at $\theta \sim 90^\circ$ and $\theta \sim 30^\circ$ with PFNS of $^{238}\text{U}(n, F)$. Even at this low incident energy PFNS shape for forward emission is much harder than that corresponding to pre-fission neutron emission at $\theta \sim 30^\circ$. Contribution of $^{238}\text{U}(n, 2nf)$ reaction to the PFNS of $^{238}\text{U}(n, F)$ is much higher than in case of $^{240}\text{Pu}(n, F)$ PFNS. Even at this low incident energy PFNS shape for forward emission is much harder than that corresponding to pre-fission neutron emission at $\theta \sim 30^\circ$.

Measurements [1, 50] encompass much lower energy range of prompt fission neutrons, than do measurements of PFNS with monochromatic neutron beams [51, 52]. That is they don't envision [50] the step-like structure due to $^{238}\text{U}(n, 2nf)^1$ neutrons [43]. Figures 10 and 11 show the partial contributions of $^{240}\text{Pu}(n, f)$, $^{240}\text{Pu}(n, nf)$ and $^{240}\text{Pu}(n, 2nf)$ contributions to $^{240}\text{Pu}(n, F)$ PFNS at $E_n \sim 17.7$ MeV at $\theta \sim 90^\circ$ and $\theta \sim 30^\circ$. The step-like structure due to $^{240}\text{Pu}(n, 2nf)^1$ neutrons is not pronounced neither at $\theta \sim 90^\circ$ or $\theta \sim 30^\circ$. Partial

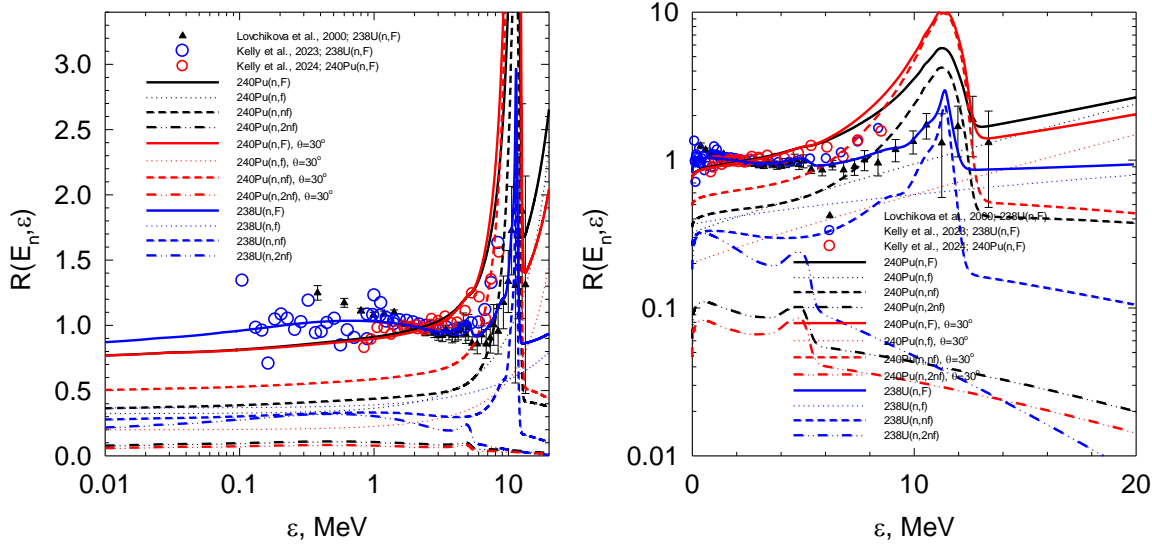


Fig.10. Ratios of partial components of PFNS of $^{240}\text{Pu}(n, F)$ at $E_n = 17.7$ MeV relative to Maxwellian type distribution with $T = 1.391867$ MeV: — — $^{240}\text{Pu}(n, F)$; ••• — $^{240}\text{Pu}(n, F)$; - - - $^{240}\text{Pu}(n, nf)$; - - • - - $^{240}\text{Pu}(n, 2nf)$; — — $^{240}\text{Pu}(n, F)$, $\theta=30^\circ$; ••• — $^{240}\text{Pu}(n, F)$, $\theta=30^\circ$; - - - $^{240}\text{Pu}(n, nf)$, $\theta=30^\circ$; - - • - - $^{240}\text{Pu}(n, 2nf)$, $\theta=30^\circ$; ○ — $^{238}\text{U}(n, F)$ [50]; ▲ — $^{238}\text{U}(n, F)$ [51, 52]; - • - — $^{238}\text{U}(n, F)$, $^{238}\text{U}(n, nf)$; ○ — $^{240}\text{Pu}(n, F)$ [1].

Fig.11. Ratios of partial components of PFNS of $^{240}\text{Pu}(n, F)$ at $E_n = 17.7$ MeV relative to Maxwellian type distribution with $T = 1.391867$ MeV: — — $^{240}\text{Pu}(n, F)$; ••• — $^{240}\text{Pu}(n, F)$; - - - $^{240}\text{Pu}(n, nf)$; - - • - - $^{240}\text{Pu}(n, 2nf)$; — — $^{240}\text{Pu}(n, F)$, $\theta=30^\circ$; ••• — $^{240}\text{Pu}(n, F)$, $\theta=30^\circ$; - - - $^{240}\text{Pu}(n, nf)$, $\theta=30^\circ$; - - • - - $^{240}\text{Pu}(n, 2nf)$, $\theta=30^\circ$; ○ — $^{238}\text{U}(n, F)$ [50]; ▲ — $^{238}\text{U}(n, F)$ [51, 52]; - • - — $^{238}\text{U}(n, F)$, $^{238}\text{U}(n, nf)$; ○ — $^{240}\text{Pu}(n, F)$ [1].

contributions of $^{238}\text{U}(n, f)$, $^{238}\text{U}(n, nf)$ and $^{238}\text{U}(n, 2nf)$ contributions to $^{238}\text{U}(n, F)$ PFNS at $E_n \sim 17.7$ MeV at $\theta \sim 90^\circ$ are much different, than those of $^{240}\text{Pu}(n, F)$ reaction. The hardening of $\langle E \rangle$ at $\theta \sim 30^\circ$ is due to

$$\text{increase of second chance fission contribution and hardening of } \frac{d^2 \sigma_{n, nf}^1(\varepsilon, E_n, \theta)}{d\varepsilon d\theta}.$$

Angular distribution of $^{239}\text{Pu}(n, xnf)$ pre-fission neutrons at $E_n \sim 14-18$ MeV, retrieved in [17] from $^{239}\text{Pu}(n, F)$, was interpreted in [9, 10]. Estimate of pre-fission neutrons contribution in [17] obtained as a difference of observed PFNS and some simple estimate of post-fission neutrons evaporated from fission fragments of $^{239}\text{Pu}(n, xnf)$ reactions. Though the procedure adopted in [17] is susceptible to systematic uncertainties, since post-fission neutrons emerge from any of $^{239}\text{Pu}(n, xnf)$ reaction, it seems hidden normalizations were used in [17]. It seems the normalization was accomplished in the energy range $\varepsilon > E_{n, f1}$. Figures 1 and 2 show the influence of forward and backward neutron emission on PFNS and average PFNS energies at $E_n \geq 12$ MeV.

Fig. 1 shows $R^{\text{exp}}(\varepsilon, E_n, \Delta\theta, \Delta\theta^1)$ of $^{239}\text{Pu}(n, F)$ PFNS and calculated ratios of $R(\varepsilon, E_n, \Delta\theta, \Delta\theta^1)$ for $^{240}\text{Pu}(n, F)$ and $^{239}\text{Pu}(n, F)$, lumped contributions of $E_n \sim 15-17.5$ MeV and $\Delta\theta \sim 35^\circ-40^\circ$ (forward direction) and $\Delta\theta^1 = 130^\circ-140^\circ$ (backward direction)

$$R(\varepsilon, 15 \div 17.5) \approx \frac{\int_{17.5}^{17.5} v_p(E_n, \approx 30^\circ) \sigma_{n, F}(E_n, \approx 30^\circ) S(\varepsilon, E_n, \theta \approx 30^\circ) \varphi(E_n) dE_n}{\int_{15}^{17.5} v_p(E_n, \theta \approx 135^\circ) \sigma_{n, F}(E_n, \theta \approx 135^\circ) S(\varepsilon, E_n, \theta \approx 135^\circ) \varphi(E_n) dE_n}, \quad (16)$$

here $\varphi(E_n)$ is the incident neutron spectrum, which is unknown. Spectra $S(\varepsilon, E_n, \theta)$ normalized to unity. As a first order approximation $R(\varepsilon, 15 \div 17.5)$ calculated as a ratio of $\nu_p(E_n, \theta)\sigma_{nF}(E_n, \theta)S(\varepsilon, E_n \approx 15-17.5, \Delta\theta) / \nu_p(E_n, \theta)\sigma_{nF}(E_n, \theta)S(\varepsilon, E_n \approx 15-17.5, \Delta\theta^1)$ for $E_n \sim 15$ MeV, $E_n \sim 16$ MeV, $E_n \sim 17$ MeV and $E_n \sim 17.5$ MeV. Values of $\nu_p(E_n, \theta)$ and $\sigma_{nF}(E_n, \theta)$ for $^{240}\text{Pu}(n, F)$ and $^{239}\text{Pu}(n, F)$ were calculated at the same energies E_n , as those in $S(\varepsilon, E_n \approx 15-17.5, \Delta\theta)$ or $R(\varepsilon, E_n, \Delta\theta, \Delta\theta^1)$. In case of angular dependent observables for $^{240}\text{Pu}(n, F)$ hidden structures in lumped $R(\varepsilon, 15 \div 17.5)$ constituents (for monochromatic beams) are smoothed. R^{exp} and $R(\varepsilon, 15-17.5)$ seem to have similar shapes, but the latter is shifted downwards. Solid line of $R(\varepsilon, 15-17.5)$ at Fig. 1 obtained by assuming in Eq. (16) equality of numerator and denominator values at $\varepsilon \sim 3-5$ MeV energy range, i.e., number of neutrons emitted in forward and backward directions, as adopted in [17]. In case of $^{240}\text{Pu}(n, F)$ and $^{239}\text{Pu}(n, F)$ at $\varepsilon > E_{\text{mf}}$, both R^{exp} and $R(\varepsilon, 15-17.5)$ values are less than unity, that might be due to influence of angular dependence of $(n, xnf)^{1,2,3}$ neutron emission on the fission chances distribution. The renormalized ratio $R(\varepsilon, E_n, \Delta\theta, \Delta\theta^1)$ of $^{239}\text{Pu}(n, F)$ seems to be consistent with reconstructed data [17], shown on Fig. 1, while that of $^{240}\text{Pu}(n, F)$ reaction is appreciably higher. Angular dependence of the first pre-fission neutron in reactions $(n, nf)^1$ and $(n, 2nf)^1$ [5, 6] helps to interpret the experimental data trend in case of ratio of average energies for “forward” and “backward” emission of pre-fission neutrons in $^{239}\text{Pu}(n, xnf)^{1,2,3}$ [17] reaction. The ratio of $\langle E(\theta) \rangle / \langle E(\theta^1) \rangle$ in case of $^{240}\text{Pu}(n, F)$ for “forward”, $\Delta\theta \sim 35^\circ-40^\circ$, and “backward”, $\Delta\theta^1 = 130^\circ-140^\circ$, emission of pre-fission neutrons also steeply increases starting from $E_n \sim 10-12$ MeV. However, for $^{240}\text{Pu}(n, F)$ PFNS the ratio of $\langle E(\theta) \rangle / \langle E(\theta^1) \rangle$ only slightly higher than in case of $^{239}\text{Pu}(n, F)$. At $E_n \sim 16$ MeV the ratio of $\langle E(\theta) \rangle / \langle E(\theta^1) \rangle$, calculated for $\varepsilon \sim 0.8-10$ MeV energy range abruptly drops. Hard pre-fission $^{240}\text{Pu}(n, nf)^1$ neutrons are responsible for that drop. When average energies calculated at energy range of $\varepsilon \sim 1-3$ MeV, ratios $\langle E(\theta) \rangle / \langle E(\theta^1) \rangle$ are virtually independent on E_n .

The ratio of average energies of exclusive neutron spectra of $^{240}\text{Pu}(n, nf)^1$, $\frac{d^2\sigma_{nf}^1(\varepsilon, E_n, \theta \approx 30^\circ)}{d\varepsilon d\theta}$ and $\frac{d^2\sigma_{nf}^1(\varepsilon, E_n, \theta \approx 135^\circ)}{d\varepsilon d\theta}$, $\langle E_{n, xnf}(\theta \approx 30^\circ) \rangle / \langle E_{n, xnf}(\theta^1 \approx 135^\circ) \rangle$, is much higher than that of $\langle E(\theta) \rangle / \langle E(\theta^1) \rangle$, however it follows the shape of experimental ratio $\langle E(\theta \approx 30^\circ) \rangle / \langle E(\theta^1 \approx 135^\circ) \rangle$ [17]. Angular dependence of the ratio of average energies of exclusive neutron spectra of $^{240}\text{Pu}(n, 2nf)^1$ $\frac{d^2\sigma_{n2nf}^1(\varepsilon, E_n, \theta \approx 30^\circ)}{d\varepsilon d\theta}$ and $\frac{d^2\sigma_{n2nf}^1(\varepsilon, E_n, \theta \approx 150^\circ)}{d\varepsilon d\theta}$ is much weaker.

6. Average total kinetic energy TKE

The excitation energy of residual nuclides, after emission of (n, xnf) neutrons, decreases by the binding energy of emitted neutron B_{nx} and its average kinetic energy as

$$U_x = E_n + B_n - \sum_{x, 1 \leq k \leq x} (\langle E_{n, xnf}^k(\theta) \rangle + B_{nx}). \quad (17)$$

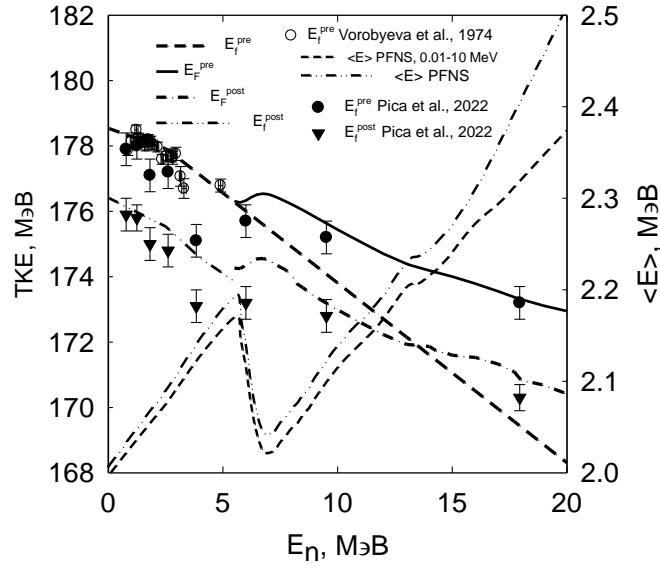


Fig. 12. Total kinetic energy TKE: $^{240}\text{Pu}(n, F)$, E_F^{pre} — — — — — ; $^{240}\text{Pu}(n, f)$, E_f^{pre} - - - - - ; $^{240}\text{Pu}(n, F)$, E_F^{post} — — • — — ; \circ — $^{240}\text{Pu}(n, F)$, E_F^{pre} [54]; \bullet — $^{240}\text{Pu}(n, F)$ E_f^{pre} [55]; \blacktriangledown — $^{240}\text{Pu}(n, F)$ E_f^{post} [55]; — — — — — , — — — — — $\langle E \rangle$ $^{240}\text{Pu}(n, F)$ in the range $\epsilon \sim 0-20$ MeV and $\epsilon \sim 0.01-10$ MeV, respectively.

The excitation energy of fission fragments is

$$E_{nx} = E_r - E_{fx}^{pre} + E_n + B_n - \sum_{x, 1 \leq k \leq x} (\langle E_{nxf}^k(\theta) \rangle + B_{nx}). \quad (18)$$

Value of TKE, kinetic energy of fission fragments prior prompt neutron emission (see Fig. 12), E_F^{pre} , is approximated by a superposition of partial TKE of $^{241-x}\text{Pu}$ nuclides as

$$E_F^{pre}(E_n) = \sum_{x=0}^X E_{fx}^{pre}(E_{nx}) \cdot \sigma_{n,nxf} / \sigma_{n,F}. \quad (19)$$

Kinetic energy of fission fragments, i.e. post-fission fragments after neutron emission (see Fig. 12), E_F^{post} , are defined as

$$E_F^{post} \approx E_F^{pre} \left(1 - \nu_{post} / (A + 1 - \nu_{pre}) \right). \quad (7)$$

Similar relation was used for E_f^{post} in [53] at $E_n < E_{mf}$.

Conclusions

Analysis of prompt fission neutron spectra of $^{240}\text{Pu}(n, F)$ evidenced correlations of a number observed data structures with $(n, xnf)^{1 \dots x}$ pre-fission neutrons. Pre-fission neutron spectra turned out to be quite soft as compared with neutrons emitted by excited fission fragments. The net outcome of that is the decrease of $\langle E \rangle$

in the vicinity of the (n, xn_f) thresholds of $^{240}\text{Pu}(n, F)$. The amplitude of the $\langle E \rangle$ variation is much higher in case of $^{240}\text{Pu}(n, F)$ as compared with $^{239}\text{Pu}(n, F)$. The correlation of PFNS shape with different angles of emission of $(n, xn_f)^1$ neutrons and emissive fission contributions for $^{240}\text{Pu}(n, F)$ is established. The angular anisotropy of exclusive pre-fission neutron spectra strongly influences the PFNS shapes and their average energies $\langle E \rangle$. These peculiarities are due to differing emissive fission (n, xn_f) contributions in $^{239}\text{Pu}(n, F)$ and $^{240}\text{Pu}(n, F)$. Calculated ratio of $\langle E \rangle$ for “forward” and “backward” emission of pre-fission neutrons steeply increases with the increase of average energies of exclusive pre-fission neutron spectra $^{240}\text{Pu}(n, xn_f)^{1\dots x}$.

The calculated anisotropy of pre-fission neutrons of $^{240}\text{Pu}(n, xn_f)$ reaction is a bit higher than in case of $^{239}\text{Pu}(n, F)$. That might be due to correlation of anisotropy of pre-fission neutrons with contribution of emissive fission (n, nf) to the observed fission cross section, PFNS and angular anisotropy of NES. In case of $^{240}\text{Pu}(n, F)$ and $^{239}\text{Pu}(n, F)$ at $\varepsilon > E_{nff1}$, both R^{exp} and $R(\varepsilon, 15 - 17.5)$ are less than unity, that also might be due to influence of angular dependence of (n, xn_f) neutron emission on the fission chances distribution.

References

1. K. J. Kelly, M. Devlin, J.M. O’Donnell et al. Phys. Rev. C, 109 (2024) 6064611(14).
2. K. J. Kelly, M. Devlin, J.M. O’Donnell et al. LANSCE Status of the measurements of $^{240}\text{Pu}(n, F)$ prompt fission neutron spectrum on LANSCE (ND1). LA-UR-23-21670. 2023; NCSP Technical Program Review (2/23/2023)
3. K. J. Kelly, M. Devlin, J.M. O’Donnell et al. Nuclear Data Week(s) 2023 (CSEWG-USNDP-NDAG), November, 2023; <https://indico.bnl.gov/event/18701/contributions/82692/>; LA-UR-23-33042.
4. K. J. Kelly, J. Gomez, M. Devlin et al. Nuclear Data Week(s) 2022 (CSEWG-USNDP-NDAG) (31 October — 11 November, 2022), <https://indico.bnl.gov/event/15497/contributions/69818/>.
5. V.M. Maslov, 30th International Seminar on Interaction of Neutrons with Nuclei: April 14 - 18, 2024, Frank’ LNP, JINR, Dubna, Russia at Sharm El-Sheikh, Egypt; http://isinn.jinr.ru/past-isinns/isinn-30/presentations/68_Maslov.zip
6. V.M. Maslov, Physics of Particles and Nuclei Letters, 20 (2023) 565.
7. B. Gerasimenko, L. Drapchinsky, O. Kostochkin et al. J. Nucl. Sci. Technol., 2 (2002) 362.
8. N.V. Kornilov, A.B. Kagalenko, F.-J. Hambsch, Yad. Fiz. 62 (1999) 209.
9. V.M. Maslov, Physics of Atomic Nuclei, 86 (2023) 627.
10. V.M. Maslov, Physics of Particles and Nuclei Letters, 20 (2023) 1401.
11. V.M. Maslov LXXIII Intern. Conf. Nucleus 2023, Fundamental problems and applications, Sarov, October, 2023, Book of Abstracts, p. 119. <http://book.sarov.ru/product/nucleus-2023-73-conference-abstracts/>; <http://book.sarov.ru/wp-content/uploads/2023/11/Nucleus-2023-73-conference-abstracts.pdf>
12. V.M. Maslov, In Proceedings of 29th International Seminar on Interaction of Neutrons with Nuclei, May 29 - June 2, 2023, Frank’ LNP, JINR, Dubna, Russia, 2023, JINR, E3-2023-58, Dubna, 2023, p.272. http://isinn.jinr.ru/proceedings/isinn-29/pdf/Maslov_1r.pdf.
13. V.M. Maslov, In Proceedings of 29th International Seminar on Interaction of Neutrons with Nuclei, May 29 - June 2, 2023, Frank’ LNP, JINR, Dubna, Russia, 2023, JINR, E3-2023-58, Dubna, 2023, p. 290. http://isinn.jinr.ru/proceedings/isinn-29/pdf/Maslov_2r.pdf;
14. V.M. Maslov, in: Proc. LXXII Intern. Conf. Nucleus 2022, Fundamental problems and applications, Moscow, 11–16 July, 2022, p. 168. https://events.sinp.msu.ru/event/8/contributions/586/attachments/568/881/mvmNucl_2022%2B.pdf
15. V.M. Maslov, in: Proc. LXXII Intern. Conf. Nucleus 2022, Fundamental problems and applications, Moscow, 11–16 July, 2022, Book of abstracts, p. 111, https://events.sinp.msu.ru/event/8/attachments/181/875_nucleus-2022-book-of-abstracts-www.pdf.
16. V.M. Maslov, Proc. 28th International Seminar on Interactions of Neutrons with Nuclei, 2021, May, 24-28, Dubna, Russia, Book of Abstracts, p. 113; <http://isinn.jinr.ru/past-isinns/isinn-28/annotations/Maslov.pdf>; <http://isinn.jinr.ru/past-isinns/isinn-28/presentations/28/Maslov.pdf>.

17. K. J. Kelly, T. Kawano, J.M. O'Donnell et al. *Phys. Rev. Lett.* 122 (2019) 072503.
18. K. J. Kelly, M. Devlin, J.M. O'Donnell et al., *Phys. Rev. C*, 102 (2020) 034615.
19. P. Marini, J. Taieb, B. Laurent et al., *Phys. Rev. C*, 101 (2020) 044614.
20. K. J. Kelly, J.A. Gomez, M. Devlin et al., *Phys. Rev. C*, 105 (2022) 044615.
21. K. Meierbachtol, F. Tovesson, D. L. Duke et al. *Phys. Rev. C*, 94 (2016) 034611.
22. A. Chemey, A. Pica, Liangyu Yao et al. *Eur. Phys. J. A.*, 56 (2020) 297.
23. J.L. Kammerdiener, UCRL-51232, 1972.
24. V.M. Maslov, Yu.V. Porodzinskij, M. Baba, A. Hasegawa, *Bull. RAS, Ser. Fyz.* 67 (2003) 1597.
25. V.M. Maslov, Yu.V. Porodzinskij, N.A. Tetereva et al., *Nucl. Phys. A*, 764 (2006) 212.
26. V.M. Maslov, M. Baba, A. Hasegawa, A. B. Kagalenko., N.V. Kornilov, N.A. Tetereva, INDC (BLR)-14, Vienna: IAEA, 2003; <https://www-nds.iaea.org/publications/indc/indc-blr-0014/>.
27. A.M. Daskalakis, R.M. Bahran, E.J. Blain et al., *Ann. Nucl. Energy*, 73 (2014) 455.
28. K. S. Mohindroo, Y. Danon, E.J. Blain et al., *Ann. Nucl. Energy*, 165 (2022) 108647.
29. M. R. Mumpower, D. Neudecker, H. Sasaki, et al., *Phys. Rev. C*, 107 (2023) 034606.
30. B.E. Watt, *Phys. Rev.* 87 (1952) 1037.
31. B. Fraïsse, G. Bélier, V. Méot et al. *Phys. Rev. C*, 108 (2023) 014610.
32. K. Shibata, O. Iwamoto, T. Nakagawa et al. *J. Nucl. Sci. Technol.*, 48 (2011) 1.
33. K. Kari and S. Cierjacks, in: *Neutron Physics and Nuclear Data for Reactors and applied purposes*, Harwell, UK, p. 905, OECD, Paris, 1978.
34. P. Staples, K. Morley, *Nucl. Sci. Eng.* 129 (1998) 149.
35. J.W. Meadows *Nucl. Sci. Eng.* 79 (1981) 233.
36. V.M. Kupriyanov, B.I. Fursov, B.K. Maslennikov et al., *Sov J. At. Energy*, 46 (1979) 35
37. J.W. Behrens, R.S. Newbury, J.W. Magana, *Nucl. Sci. Eng.* 66 (1978) 433.
38. A.B. Laptjev, A. Yu. Donetz, V.N. Dushin et al. In: *Proc. of the International Conference on Nuclear Data for Science and Technology*, September 26 – October 1, 2004, Santa Fe, USA, p. 865.
39. F. Tovesson, T.S. Hill, M. Mocko, J.D. Baker, C.A. Mcgrath, *Phys. Rev. C*, 79 (2009) 014613.
40. Yu. A. Khokhlov, I.A. Ivanin, V.I. In'kov et al. In: *Proc. Int. Conf. Nuclear Data for Science and Technology*, Gatlinburg, USA, May 9-13, 1994, p. 272, J.K. Dickens (Ed.), ANS, 1994.
41. J. Frehaut, G. Mosinski, R. Bois, M. Soleilhac, CEA-R-4626, 1974
42. B.D. Kuz'minov, *NEJTRONFIZ*, 246, 1961.
43. V.M. Maslov, Yu. V. Porodzinskij, M. Baba, A. Hasegawa, N.V. Kornilov, A.B. Kagalenko and N.A. Tetereva, *Phys. Rev. C*, 69 (2004) 034607.
44. V.M. Maslov. *Nucl. Phys. A* 743 (2004) 236.
45. V.M. Maslov, *Phys. Rev. C*, 72 (2005) 044607.
46. M. Uhl and B. Strohmaier, IRK-76/01, IRK, Vienna, 1976.
47. A. Chatillon, G. Belier, T. Granier et al. *Phys. Rev. C*, 89 (2014) 014611.
48. Yu.S. Zamyatnin, I.N. Safina, E.K. Gutnikova, N.I. Ivanova, *At. Energy*, 4 (1958) 337.
49. A.M. Trufanov, G.N. Lovchikova, M.I. Svirin et al. *Yad. Fiz.* 64 (2001) 3.
50. K. J. Kelly, M. Devlin, J.M. O'Donnell et al., *Phys. Rev. C*, 108 (2023) 024603.
51. Lovchikova GN, Trufanov AM, Svirin MI et al. In: *Proceedings of the XIV international workshop on nuclear fission physics*. Obninsk, 12–15 Oct 2000, SSC RF IPPE, Obninsk, Russia, 2000, p. 72.
52. G.N. Lovchikova, A.M. Trufanov, M.I. Svirin et al. *Yad. Fiz.* 67, 1270 (2004).
53. D. Madland, *Nucl. Phys. A* 772 (2006) 113.
54. V.G. Vorobjeva, N.P. Djachenko, B.D. Kuz'minov, *Atom. Energiya*, 36 (1974) 32.
55. A. Pica, A. T. Chemey and W. Loveland, *Phys. Rev. C*, 106 (2022) 044603.